Expanded tRNA methyltransferase family member TRMT9B regulates synaptic growth and function

Caley A Hogan[1,†] [ID], Scott J Gratz[2,†] [ID], Jennifer L Dumouchel[3,†] [ID], Rajan S Thakur[2] [ID], Ambar Delgado[2] [ID], Jenna M Lentini[4] [ID], Kimberly R Madhwani[5] [ID], Dragony Fu[4] [ID] & Kate M O'Connor-Giles[2,6,*] [ID]

Abstract

Nervous system function rests on the formation of functional synapses between neurons. We have identified TRMT9B as a new regulator of synapse formation and function in *Drosophila*. TRMT9B has been studied for its role as a tumor suppressor and is one of two metazoan homologs of yeast tRNA methyltransferase 9 (Trm9), which methylates tRNA wobble uridines. Whereas Trm9 homolog ALKBH8 is ubiquitously expressed, TRMT9B is enriched in the nervous system. However, in the absence of animal models, TRMT9B's role in the nervous system has remained unstudied. Here, we generate null alleles of *TRMT9B* and find it acts postsynaptically to regulate synaptogenesis and promote neurotransmission. Through liquid chromatography-mass spectrometry, we find that ALKBH8 catalyzes canonical tRNA wobble uridine methylation, raising the question of whether TRMT9B is a methyltransferase. Structural modeling studies suggest TRMT9B retains methyltransferase function and, *in vivo*, disruption of key methyltransferase residues blocks TRMT9B's ability to rescue synaptic overgrowth, but not neurotransmitter release. These findings reveal distinct roles for TRMT9B in the nervous system and highlight the significance of tRNA methyltransferase family diversification in metazoans.

Introduction

Complex nervous systems are composed of thousands to billions of neurons connected through synapses in neural circuits that control behavior and thought. To achieve this functional organization, neurons must form synaptic connections in appropriate numbers and strength during development. Synapse number and strength are also substrates for the neuronal plasticity that underlies experience-dependent changes to brain function (Citri & Malenka, 2008). Dysregulation of synapse formation and plasticity has been broadly linked to neurodevelopmental disorders, including intellectual disability (Zoghbi & Bear, 2012; Guang *et al*, 2018). While we have learned a great deal about a small subset of genes underlying neurodevelopmental disorders, a recent study found that the majority of genes in the human genome are understudied—including those associated with human disorders (Stoeger *et al*, 2018). With the increasingly broad application of clinical sequencing in individuals with neurodevelopmental delay, new genes whose function in the nervous system remains unknown are being uncovered. A lack of foundational understanding of synaptic gene function is a significant obstacle for translating clinical identification of causative variants into effective treatments for neurodevelopmental disorders.

To uncover conserved, uncharacterized genes with roles in the formation of functional synapses, we first looked for genes expressed "in the right place at the right time." Using ModENCODE data (Graveley *et al*, 2011; Brown *et al*, 2014), we observed that many *Drosophila* synaptic genes exhibit a unique spatiotemporal transcriptional profile during development. Expression is enriched in the nervous system and transcription is generally low with peaks during each of the two periods of extensive synaptogenesis, late embryonic and pupal (Fig EV1). We reasoned that uncharacterized genes with this expression pattern might be enriched for genes involved in synapse formation and/or function and compared the expression pattern of every gene in the genome with this profile. Focusing on genes with the highest correlation coefficients that were uncharacterized and conserved in mammals, we began generating CRISPR loss-of-function and endogenously tagged alleles to assess potential roles in synapse development at the well-characterized glutamatergic neuromuscular junction (NMJ). Computed Gene 42261 (CG42261) emerged as a potential negative regulator of synaptic growth. CG42261, which was also identified in an RNAi screen as a potential

1 Genetics Training Program, University of Wisconsin-Madison, Madison, WI, USA
2 Department of Neuroscience, Brown University, Providence, RI, USA
3 Therapeutic Sciences Graduate Program, Brown University, Providence, RI, USA
4 Department of Biology, Center for RNA Biology, University of Rochester, Rochester, NY, USA
5 Neuroscience Graduate Training Program, Brown University, Providence, RI, USA
6 Carney Institute for Brain Science, Providence, RI, USA
   *Corresponding author. Tel: +1 401 863 3610; E-mail: oconnorgiles@brown.edu
   †These authors contributed equally to this work

regulator of thermal nociception and named *fire dancer* (Honjo *et al*, 2016), encodes the *Drosophila* homolog of human TRMT9B. TRMT9B has been studied for its role as a tumor suppressor and is downregulated in colorectal, breast, bladder, cervical, ovarian, and testicular carcinomas (Flanagan *et al*, 2004; Begley *et al*, 2013; Chen *et al*, 2017; Wang *et al*, 2018). TRMT9B is one of two metazoan homologs of yeast tRNA methyltransferase 9 (Trm9), which methylates tRNA wobble uridines (Kalhor & Clarke, 2003; Begley *et al*, 2007, 2013; Songe-Moller *et al*, 2010; Fu *et al*, 2010a). Trm9 homolog ALKBH8 has a demonstrated role in catalyzing tRNA wobble uridine methylation in mammals (Songe-Moller *et al*, 2010; Fu *et al*, 2010a), whereas it has remained unknown if TRMT9B plays a similar role despite years of study. Intriguingly, an emerging body of work demonstrates that enzymes in the expanded metazoan tRNA methyltransferase family have evolved to methylate new substrates, including rRNAs, mRNAs, and proteins (Chen *et al*, 2011; Abbasi-Moheb *et al*, 2012; Xu *et al*, 2017; Chellamuthu & Gray, 2020). Methylation of each of these substrates provides a reversible level of regulation that modulates biological processes ranging from transcription to splicing to translation to protein interactions, pointing to diverse regulatory roles for tRNA methyltransferase family members (Murn & Shi, 2017; Greenberg & Bourc'his, 2019; Zhou *et al*, 2020).

Here, we detail the first animal model of *TRMT9B* to investigate its biological role in the nervous system. Using endogenously tagged lines, we find that TRMT9B is expressed in neuronal, glial, and muscle cell bodies and at synapses. At the NMJ, TRMT9B functions postsynaptically to regulate synaptic growth and promote neurotransmitter release. Through quantitative RNA mass spectrometry, we determined that TRMT9B is dispensable for baseline tRNA wobble uridine methylation, raising the possibility that it has evolved a new function. Our modeling studies and genetic rescue experiments suggest that TRMT9B regulates synapse formation through a methyltransferase-dependent mechanism whereas its role in neurotransmission appears to be independent of enzymatic function. Together our findings highlight the expanding roles of the tRNA methyltransferase family in animals and reveal critical requirements for TRMT9B in nervous system development.

Results

TRMT9B negatively regulates synaptic growth

As part of an ongoing effort to identify and characterize new regulators of synapse formation and function, we used ModENCODE developmental RNA-Seq data to identify uncharacterized, conserved neuronal genes whose expression in *Drosophila* corresponds to periods of synaptogenesis (Graveley *et al*, 2011). We then began generating CRISPR alleles of top candidate genes and investigating synapse number at glutamatergic motor synapses. As detailed below, loss of CG42261, which encodes one of two *Drosophila* homologs of yeast wobble uridine methyltransferase Trm9, resulted in significant ectopic synapse formation. CG42261 was also identified in an RNAi screen for candidate regulators of thermal nociception and named *fire dancer (fid)*; (Honjo *et al*, 2016). Here, we follow recently established nomenclature for members of the tRNA

methyltransferase family and refer to CG42261/Fid as TRMT9B (Tweedie *et al*, 2021).

We used CRISPR-based gene editing to generate two independent null alleles: (i) $TRMT9B^{KO}$, in which the exons coding for 1366 out of 1391 amino acids are removed and replaced with a visible marker and attP landing site and (ii) $TRMT9B^{HA+IC}$, in which an HA peptide tag and a cassette encoding a visible marker flanked by piggyBac inverted terminal repeat sequences are inserted after the sole *TRMT9B* translational start site (Fig 1A). The visible marker cassette disrupts the open reading frame to generate a null allele, and its subsequent removal by piggyBac transposase yields an in-frame epitope-tagged allele (Bruckner *et al*, 2017; Gratz *et al*, 2019).

At well-characterized *Drosophila* larval NMJs, individual motor neurons from tens to hundreds of glutamatergic synapses with postsynaptic muscle targets in a stereotyped manner. We quantified synaptic growth by counting synaptic boutons at the highly stereotyped NMJ 4 formed between motor neuron 4-1b and muscle 4. We observed a significant increase in bouton number in homozygous $TRMT9B^{KO}$, homozygous $TRMT9B^{HA+IC}$, and heteroallelic $TRMT9B^{KO/HA+IC}$ mutants (Fig 1B–E, and G). All three *TRMT9B* allelic combinations exhibited a 30–35% increase in bouton number relative to control. We observe similar synaptic overgrowth in $TRMT9B^{KO}$ over a deficiency and in a line with artificial stop codons ($TRMT9B^{MiMIC-STOP}$) that is partially restored to wild type when one copy of the stop cassette is replaced with GFP ($TRMT9B^{MiMIC-GFP}$, Fig EV2A; Venken *et al*, 2011; Nagarkar-Jaiswal *et al*, 2015). We also observe synaptic overgrowth at NMJ 6/7 (Fig EV2B), consistent with a broader role in restraining synapse formation.

To further confirm the loss of *TRMT9B* as the cause of synaptic overgrowth, we restored gene function under endogenous control by removing the interfering cassette in $TRMT9B^{HA+IC}$ to generate N-terminally tagged $TRMT9B^{HA}$. Bouton number at $TRMT9B^{HA}$ NMJs was restored to near control levels, suggesting the endogenous tag may have a minor effect on protein function (Fig 1F and G). Together, these findings reveal a requirement for TRMT9B in restraining synaptic growth.

TRMT9B promotes neurotransmitter release

To investigate the impact of loss of TRMT9B on nervous system function, we assessed neurotransmission at *TRMT9B* null NMJs. To assess neurotransmission in our mutants, we measured spontaneous and evoked synaptic potentials through current clamp recordings at muscle 6, which is innervated by one type Ib and one type Is motor neuron. We observed significantly reduced excitatory junction potentials (EJPs) together with normal miniature EJP (mEJP) amplitude (quantal size) in *TRMT9B* null mutants (Fig 2A–E). These findings indicate a 51% decrease in neurotransmitter release (quantal content; Fig 2F). Restoration of endogenous *TRMT9B* function through removal of the $TRMT9B^{HA+IC}$ interfering cassette fully rescued EJPs (Fig 2C and D, $TRMT9B^{HA}$). mEJPs were slightly increased and quantal content was not fully restored to wild-type levels (Fig 2C, E, and F), suggesting again that the endogenous tag may have a small effect on TRMT9B function. Thus, in addition to its role in restraining synaptic growth, TRMT9B promotes synaptic function.
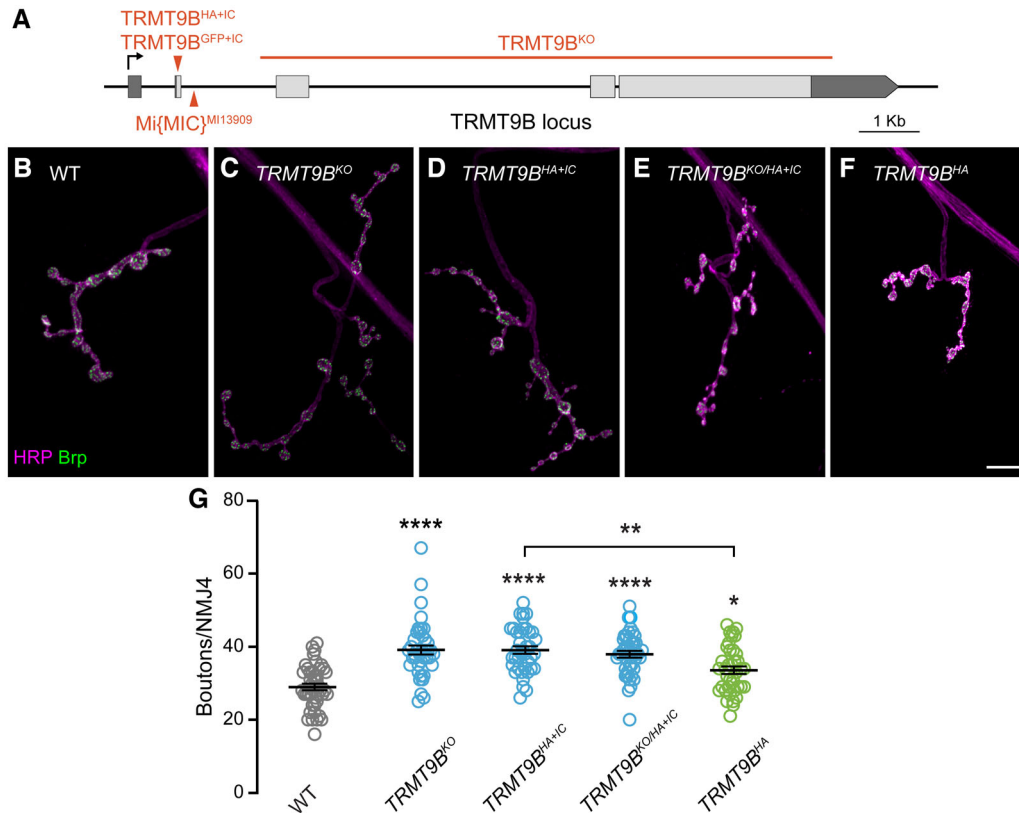
Figure 1. TRMT9B attenuates synaptic growth.

A   Schematic of the *TRMT9B* locus with alleles used in this study. Red triangles represent insertion alleles and the red line delineates the extent of the deletion in the *TRMT9B*[KO].

B–F   Representative confocal images of NMJ4 in wild type (gray), three allelic combinations of *TRMT9B* null mutants (blue), and rescue (green). Scale bar: 10 μm.

G   Quantification of bouton number per NMJ4 from B-F. Data points represent individual NMJs (*w*[1118]: 44, *TRMT9B*[KO]: 40, *TRMT9B*[HA+IC]: 39, *TRMT9B*[KO/HA+IC]: 42; *TRMT9B*[HA]: 39) from 8 to 10 biological replicates per genotype. Mean ± S.E.M. is indicated. Kruskal–Wallis test followed by Dunn's multiple comparisons test. ****$P < 0.0001$, **$P = 0.004$, *$P = 0.034$.

TRMT9B is expressed in neurons, glial, and muscle

Consistent with its roles in synapse development, *TRMT9B* is enriched in *Drosophila* and mammalian nervous systems in contrast to ALKBH8, which is ubiquitously expressed across species (Brown *et al*, 2014; Yue *et al*, 2014; GTEx, 2015; Uhlén *et al*, 2015). To investigate the cellular and subcellular expression of TRMT9B in the nervous system and at the NMJ, we turned to our endogenously tagged alleles. In N-terminally tagged *TRMT9B*[sfGFP], we observe expression in neuronal cell bodies (Fig 3A) and the synaptic neuropil of the larval ventral ganglion as indicated by colocalization with active zone protein Brp (Fig 3B). To determine which cell types express TRMT9B in the nervous system, we conducted colocalization studies with the neuronal marker Elav and glial marker Repo. We found that TRMT9B is strongly expressed in neuronal as well as glial cell bodies (Fig 3C). TRMT9B is also expressed in muscle, where it is broadly cytoplasmic with perinuclear accumulation (Fig 3D). Finally, we observe TRMT9B at the NMJ where it primarily colocalizes presynaptically with the neuronal membrane marker HRP. In contrast, we do not observe expression at the postsynaptic density (Fig 3D). While we cannot rule out the possibility that the tag has a minor effect on subcellular localization, we observe a similar expression pattern, albeit at lower levels, in *TRMT9B*[HA], which largely rescues synaptic growth and function (see Figs 1 and 2, and EV3A–C), indicating that tagged alleles localize similarly in the nervous system. TRMT9B's broad cellular and subcellular expression pattern in neurons, glial, and muscle raises the intriguing possibility of a role for TRMT9B in methylating different substrates in distinct cells and subcellular locations, including at synapses.

TRMT9B functions postsynaptically to regulate synaptic growth

Synapse formation involves a complex interplay between pre- and postsynaptic cells, both of which express TRMT9B. Our endogenous rescue system offers the advantage of driving expression at biological levels, but does not allow spatial control of gene expression. To determine the site of TRMT9B function in regulating motor synapse formation, we conducted cell-specific rescue using *C155-Gal4* and *24B-Gal4* to drive the expression of a full-length *TRMT9B* transgene in presynaptic neurons and postsynaptic muscle, respectively. We found that muscle, but not neuronal, expression of *TRMT9B* fully rescues synaptic growth at the NMJ (Fig 4A–H). Thus, TRMT9B acts postsynaptically to attenuate synaptic growth.
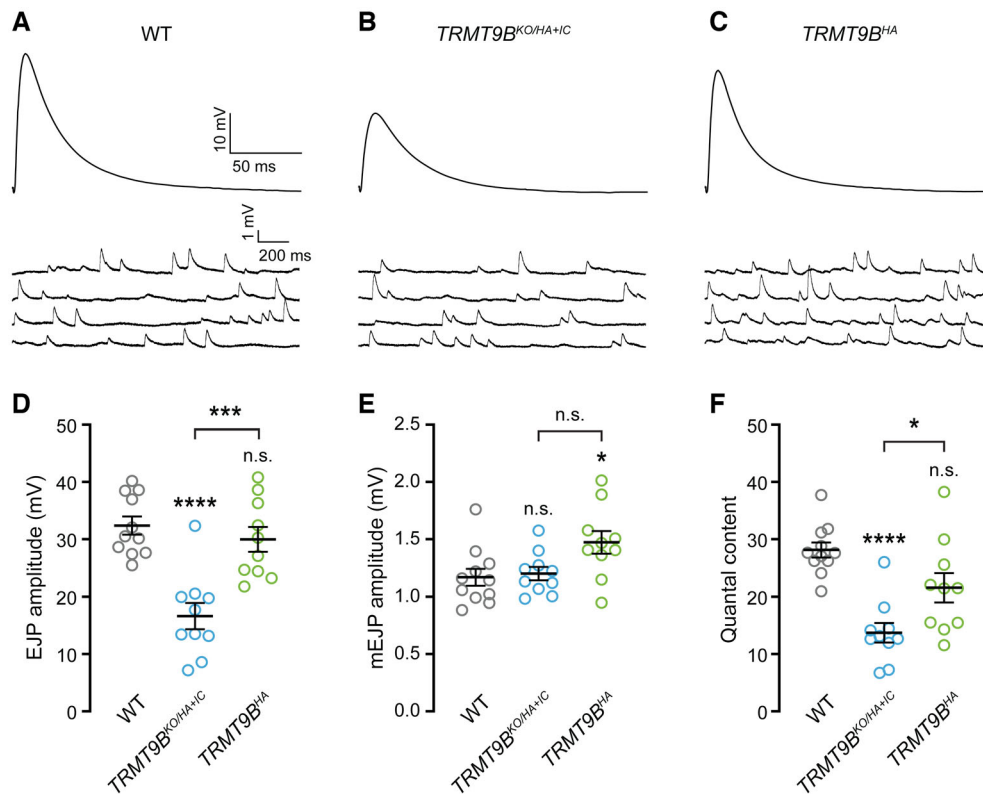
Figure 2. TRMT9B promotes neurotransmitter release.

A–C Representative traces of EJPs and mEJPs from current clamp recordings at muscle 6 in wild type (gray), *TRMT9B* null (blue), and rescue (green). Stimulus artifacts have been removed from EJPs for clarity.

D–F Quantification of average mEJP amplitude, EJP amplitude, and quantal content for genotypes in (A–C). Data points represent individual NMJs (w^{1118}: 11, *TRMT9B*$^{KO/HA+IC}$: 10; *TRMT9B*^{HA}: 10) from 5 to 8 biological replicates per genotype. Mean ± S.E.M. is indicated. ANOVA followed by Tukey's test. ****$P < 0.0001$, ***$P = 0.0002$, *$P < 0.05$.

We next quantified individual active zones labeled with Brp and found that the number of active zones per NMJ is wild type in *TRMT9B* mutants due to a decrease in active zone number per bouton that offsets the increase in bouton number (Fig 4I–L). This indicates that a previously described homeostatic mechanism for maintaining overall active zone number at NMJs (Goel *et al*, 2019) is intact in the absence of TRMT9B. Coupled with the decrease in neurotransmitter release, this further suggests that individual *TRMT9B* synapses are impaired. Thus, TRMT9B regulates both NMJ growth and the formation of functional synapses—defining fundamental neurodevelopmental roles for this member of the expanded family of metazoan tRNA methyltransferases.

Wobble uridine methylation in the absence of TRMT9B

We next sought to determine whether TRMT9B retains canonical tRNA methyltransferase function. Both TRMT9B and its paralog ALKBH8 are homologous to yeast Trm9, yet it has remained unknown whether both proteins methylate wobble uridines. Of the two metazoan homologs, TRMT9B has a domain structure more similar to Trm9 with a well-conserved Class I SAM-dependent methyltransferase domain (Fig 5A). In contrast, ALKBH8, in addition to a conserved methyltransferase domain, contains an RNA-binding motif and a 2OG-Fe (II) oxygenase domain that catalyzes an animal-specific tRNA modification (Fig 5A; Fu *et al*, 2010b; van den Born *et al*, 2011). Mouse and human ALKBH8 have been shown to methylate tRNA wobble uridines (Songe-Moller *et al*, 2010; Fu *et al*, 2010a), whereas TRMT9B's biochemical function has remained unknown in the absence of animal models. To investigate the respective roles of the two *Drosophila* Trm9 paralogs in tRNA methylation, we generated a null allele of *Drosophila ALKBH8*, currently identified as CG17807. To our knowledge, this is the first animal model in which both paralogs have been knocked out, allowing us to investigate the molecular function of each protein.

Most of our understanding of tRNA wobble uridine modification comes from studies of Trm9 in yeast (Schaffrath & Leidel, 2017). In one branch of the wobble uridine modification pathway, the Elongator complex is thought to act first to generate 5-carbonylmethyluridine (cm5U, Fig 5B, purple). Trm9 then acts in concert with obligate cofactor Trm112 to add a second methyl group and generate 5-methoxycarbonylmethyluridine (mcm5U, Fig 5B, pink). Further modification by the Ncs2-Ncs6 thiolase complex generates a terminal mcm5s2U modification (Fig 5B, green). In a second branch, wobble uridines in certain tRNAs are converted to the amide modification ncm5U by an unknown enzyme (Fig 5B, orange Johansson *et al*, 2008).
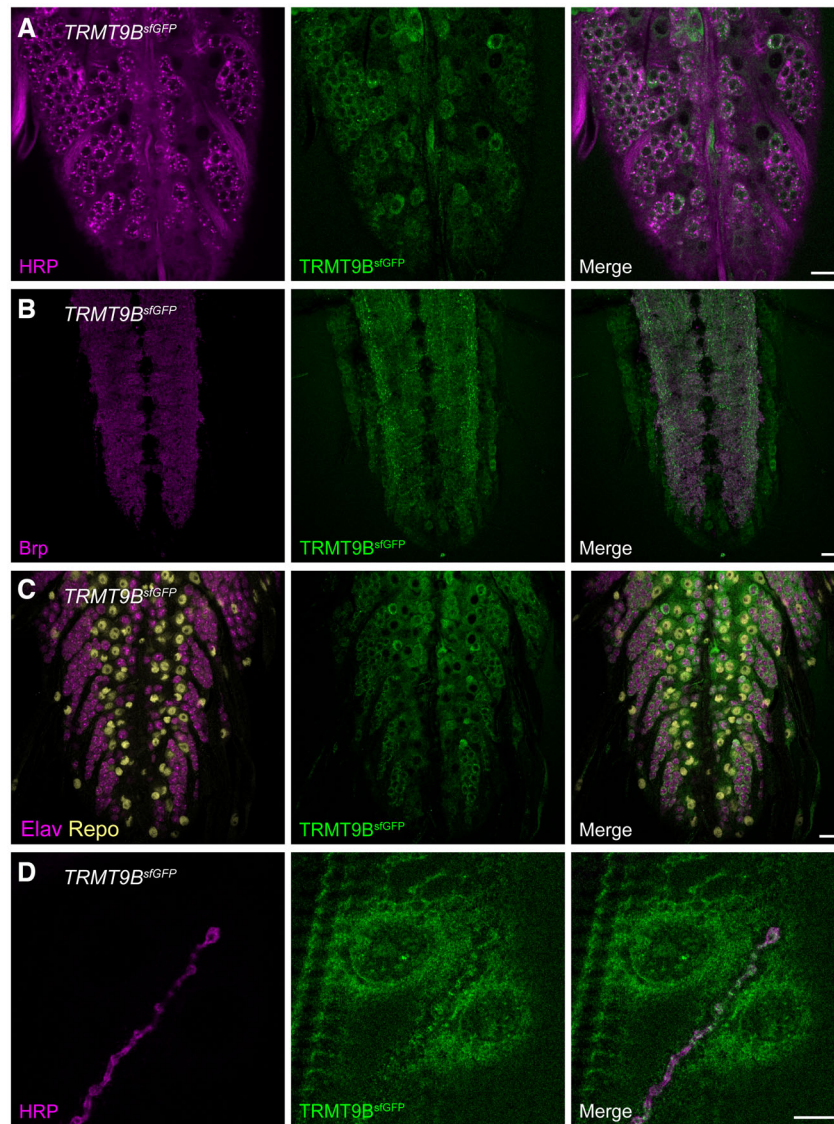
Figure 3. TRMT9B is expressed in neuronal, glial, and muscle cell bodies and at synapses.

A Confocal Z-projections of a *TRMT9B^{sfGFP}* larval ventral ganglion co-labeled with antibodies against GFP (green) and the neuronal membrane marker HRP (magenta) showing expression in cell bodies.

B Confocal Z-projections of a *TRMT9B^{sfGFP}* larval ventral ganglion co-labeled with antibodies against GFP (green) and the synaptic marker Brp (magenta) showing expression in the synaptic neuropil.

C Confocal Z-projections of a *TRMT9B^{sfGFP}* larval ventral ganglia co-labeled with antibodies against GFP (green), neuronal marker Elav (magenta), and glial marker Repo (yellow) showing expression in neurons and glia.

D Confocal Z-projections of a *TRMT9B^{sfGFP}* NMJ/muscle co-labeled with antibodies against GFP (green) and neuronal membrane marker HRP (magenta) showing expression in boutons and muscle with perinuclear accumulation. Scale bars for (A–D): 10 μm.

To analyze tRNA wobble uridine modification in our null alleles, we conducted quantitative liquid chromatography-mass spectrometry (LC–MS). Briefly, total RNA isolated from heads of mated male and female control, *TRMT9B^{KO}*, and *ALKBH8^{KO}* flies was nuclease digested and dephosphorylated to generate individual ribonucleosides followed by LC–MS analysis of nucleoside modifications (Fu *et al*, 2010a; Cai *et al*, 2015; Dewe *et al*, 2017). We found that the mcm5s2U modifications, which are tRNA specific and in yeast depend on Trm9, are present in nucleosides isolated from control

and *TRMT9B^{KO}* flies, but reduced to near background levels in *ALKBH8^{KO}* flies (Fig 5C). Similarly, mcm5U, which is the terminal modification for a single tRNA and thus present at low levels near our resolution of detection, was observed at similar levels in control and *TRMT9B^{KO}* flies (control: 92.13 ± 14.59, *TRMT9B^{KO}*: 101.70 ± 26.45, $P = 0.92$) and not detected in the absence of ALKBH8. Notably, we detected an increase in the accumulation of ncm5U and ncm5S2U in *ALKBH8^{KO}* flies, but not control or *TRMT9B* flies (Fig 5C and D). These findings are consistent with studies in yeast,
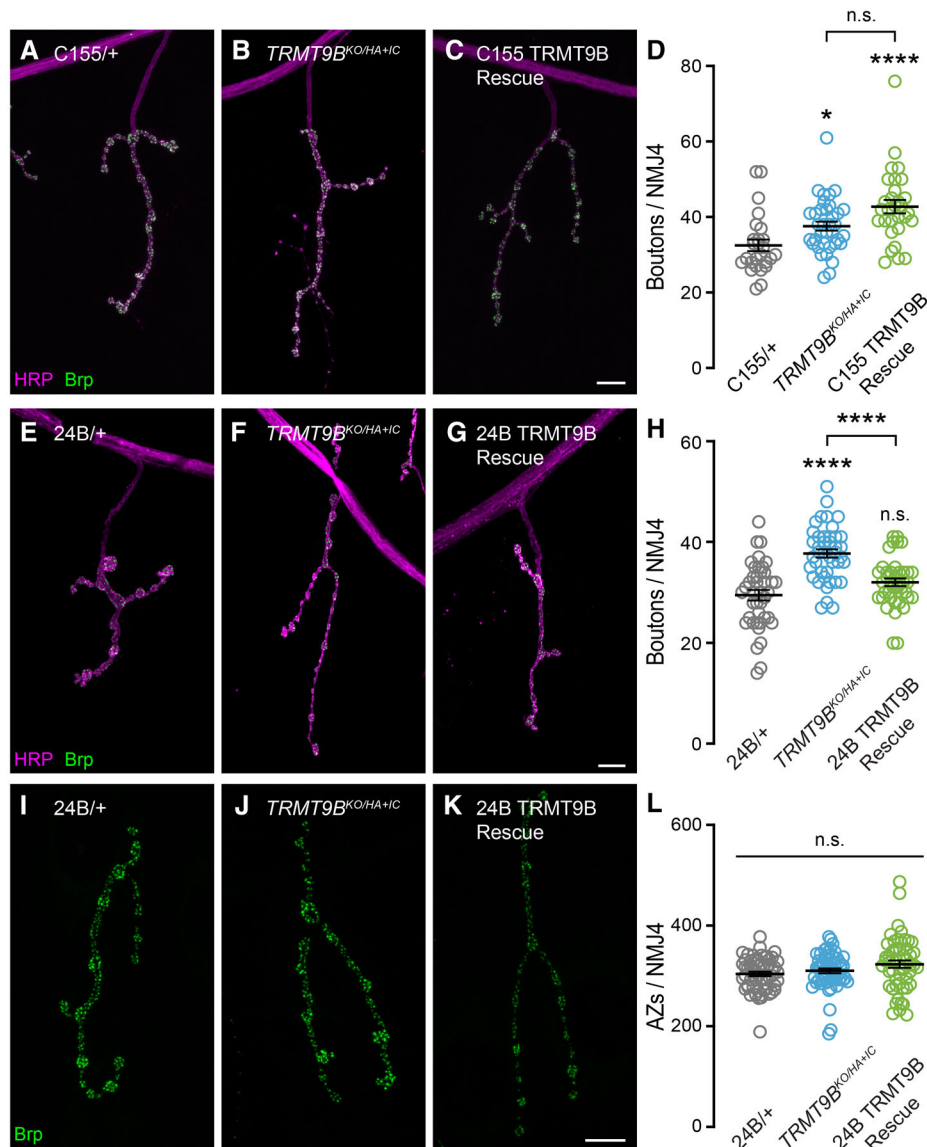
Figure 4. TRMT9B functions postsynaptically to regulate synaptic growth.

A–C   Representative confocal images of NMJ4 in control (gray), *TRMT9B* null (blue), and presynaptic rescue (green).
D   Quantification of bouton number per NMJ4 from (A–C). Data points represent individual NMJs (*C155 Gal4/+*: 26, *C155 Gal4/+*; *TRMT9B^{KO/HA+IC}*: 36; *C155-Gal4*; *TRMT9B^{KO}/UAS-TRMT9B, TRMT9B^{HA+IC}*: 30) from 10 biological replicates per genotype.
E–G   Representative confocal images of NMJ4 in control (gray), *TRMT9B* null (blue), and postsynaptic rescue (green).
H   Quantification of bouton number per NMJ4 from E–G. Data points represent individual NMJs (*24B-Gal4/+*: 41, *24B-Gal4, TRMT9B^{KO/HA+IC}*: 42; *24B-Gal4, TRMT9B^{KO}/UAS-TRMT9B, TRMT9B^{HA+IC}*: 40) from 8 to 10 biological replicates per genotype.
I–K   Representative high-resolution confocal images of NMJs with individual active zones labeled with Brp in control (gray), *TRMT9B* null (blue), and postsynaptic rescue (green).
L   Quantification of active zone (AZ) number per NMJ4 from I-K. Data points represent individual NMJs (*24B-Gal4/+*: 59, *24B-Gal4/+, TRMT9B^{KO/HA+IC}*: 59; *24B-Gal4, TRMT9B^{KO}/UAS-TRMT9B, TRMT9B^{HA+IC}*: 53) from 10 biological replicates per genotype.

Data information: Mean ± S.E.M. is indicated. Kruskal–Wallis test followed by Dunn's multiple comparisons test. ****$P < 0.0001$, *$P = 0.02$. Scale bars: 10 μm.

showing that loss of Trm9 leads to loss of mcm5s2U concomitant with the accumulation of amide intermediates (Chen *et al*, 2011). Based on these findings, we conclude that ALKBH8 methylates tRNA wobble uridines independently of TRMT9B under basal conditions.

We next explored the possibility that TRMT9B catalyzes a different tRNA methylation—a possibility hinted at in previous overexpression studies (Begley *et al*, 2013). Specifically, we investigated a panel of well-characterized tRNA modifications at multiple tRNA sites, the majority involving methylation. Further confirming our results above, we found that mcm5s2U was decreased to near background levels in *ALKBH8^{KO}* flies while no major change in mcm5s2U was detected in *TRMT9B^{KO}* flies (Fig 5D). For the remaining modifications with levels within a quantifiable range, we

observed a slight variation in levels for a subset of nucleosides iso-lated from the *ALKBH8*^KO flies when compared to control flies, suggesting that loss of ALKBH8-catalyzed wobble uridine modifications could impact other tRNA modifications. In contrast, no modification exhibited more than a two fold change in the *TRMT9B*^KO compared with control.
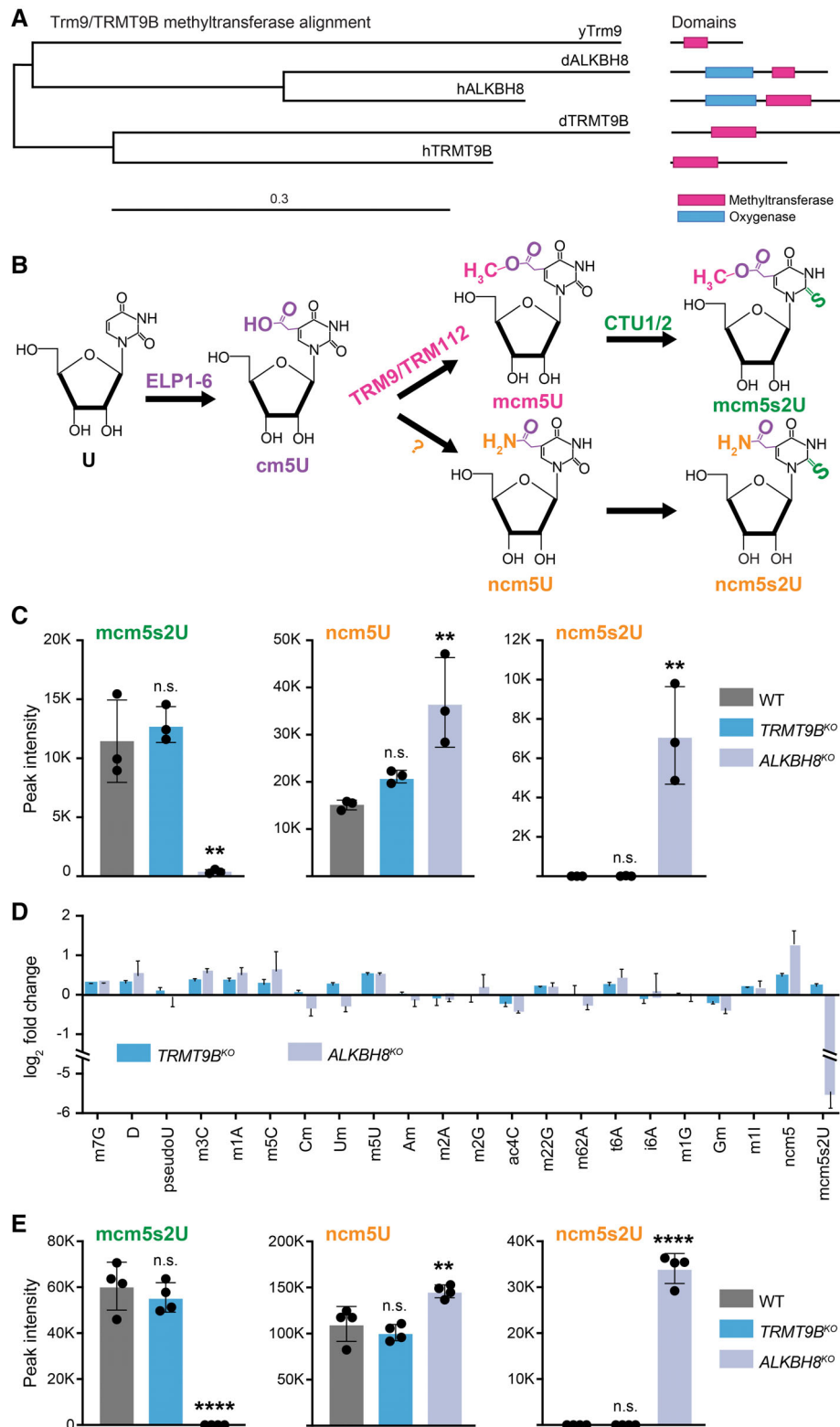

Figure 5.

◀

Finally, we explored the possibility that TRMT9B has a developmental role in tRNA wobble uridine modification by analyzing wobble uridine modifications in third-instar larvae. We isolated the nervous system and body walls to assess both neuronal and muscle roles. Again, we found that mcm5s2U is lost while ncm5U and ncm5S2U are increased in *ALKBH8*, but not *TRMT9B*, mutants (Fig 5E). While our findings do not rule out the possibility that TRMT9B plays a conditional role in tRNA wobble uridine methylation or methylates a small subset of tRNAs not detectable by bulk analysis, these observations indicate that ALKBH8 is the primary paralog carrying out the canonical Trm9 tRNA wobble uridine methyltransferase role and suggest a new role for TRMT9B.

TRMT9B has a structurally conserved methyltransferase domain

Our LC-MS findings raise the question of whether TRMT9B has maintained function as a methyltransferase or evolved a nonenzymatic role. To investigate TRMT9B's potential role as a methyltransferase, we first aligned the predicted methyltransferase domains of yeast Trm9 with *Drosophila* and human TRMT9B (Fig 6A). Although methyltransferases are not generally well conserved at the level of primary sequence (Martin & McMillan, 2002), we observe conservation throughout the methyltransferase domain, including residues known to be important for methyltransferase function. The defining sequence features of Class I SAM-dependent methyltransferase are (i) an acidic residue at the end of the first beta strand and (ii) a GxGxG SAM-binding motif—both of which are critical for SAM binding and conserved in yeast Trm9 and fly and human TRMT9B (Fig 6A, blue boxed residues; Martin & McMillan, 2002; Kozbial & Mushegian, 2005). Additional acidic residues in beta strands 2, 3, and 4 and glycines in beta strand 5 that are highly conserved across Class I SAM-dependent methyltransferases are also present in fly and human TRMT9B (Fig 6A, blue residues; Kozbial & Mushegian, 2005). We next assessed residues found to be critical for SAM binding and enzymatic activity in a comprehensive mutational analysis of yeast Trm9 (Létoquart *et al*, 2015) and found that these residues are highly conserved in *Drosophila* and human TRMT9B (Fig 6A, black and red boxed residues) as well as ALKBH8. Together, these observations are consistent with the model that both paralogs retain methyltransferase function.

To investigate tertiary structure, we generated structural homology models of the methyltransferase domains of *Drosophila* and human TRMT9B and ALKBH8. For an unbiased approach, we used Modeller to model the methyltransferase domains against known crystal structures reported in the RCSB Protein Data Bank (Pieper *et al*, 2014) and identified Trm9 as a match for each enzyme, lending further support for the hypothesis that both TRMT9B and ALKBH8

maintain methyltransferase function. To evaluate structural conservation, we used Chimera to compare our *Drosophila* TRMT9B methyltransferase domain model to the yeast Trm9 structure determined by X-ray diffraction of *Yarrowia lipolytica* Trm9 and its obligate cofactor Trm112 (Fig 6B; Létoquart *et al*, 2015). Class I methyltransferases form a seven-stranded beta sheet flanked by alpha helices. In our model, this folded structure is maintained and key residues are superimposed (Fig 6B, orange ribbon). We observed similar structural conservation between yeast Trm9 and our model of human TRMT9B (Fig EV4A). We next overlaid our models of TRMT9B with *Drosophila* and human ALKBH8 and observed significant structural conservation between the four methyltransferase domains (Fig 6C). Finally, we assessed the predicted structure of the *Drosophila* TRMT9B methyltransferase domain using AlphaFold (Jumper *et al*, 2021; Varadi *et al*, 2022). Strong alignment was observed between the AlphaFold predicted model, the *Drosophila* TRMT9B model predicted using Modeller, and the yeast Trm9 crystal structure (Fig EV4B). Thus, multiple independent *in silico* modeling approaches support structural conservation of TRMT9B's methyltransferase domain across species, suggesting TRMT9B functions as a methyltransferase in flies and humans.

Disruption of TRMT9B's methyltransferase domain blocks rescue of synaptic growth

To experimentally determine whether TRMT9B functions as a methyltransferase, we sought to generate a methyltransferase-dead rescue construct for expression under GAL4 control and compare its ability to rescue synaptic growth deficits in *TRMT9B* mutants to wild-type rescue constructs. To disrupt methyltransferase function, we replaced two residues identified by Létoquart *et al* (2015) as critical for SAM substrate binding and catalytic activity in Trm9 with alanines (see Fig 6A, red boxed residues; Létoquart *et al*, 2015). Absent a known substrate for TRMT9B, we cannot biochemically assess the disruption of methyltransferase function, so we confirmed that the residues correspond in our structural alignments and modeled the effect of alanine substitutions on protein structure to confirm that tertiary protein structure remains intact, consistent with prior studies (Fig 7A; Létoquart *et al*, 2015). We integrated wild-type (*UAS-TRMT9B*) and methyltransferase-dead (*UAS-TRMT9B^{MTD}*) transgenes at the same genomic site and expressed each transgene under the control of *24B-Gal4* in *TRMT9B* nulls. While expression of wild-type *TRMT9B* fully rescued synaptic overgrowth as observed above, expression of *TRMT9B^{MTD}* failed to rescue (Fig 7B–F), consistent with the conclusion that methyltransferase activity is required for TRMT9B's role in regulating synaptic growth. To confirm proper translation and localization of
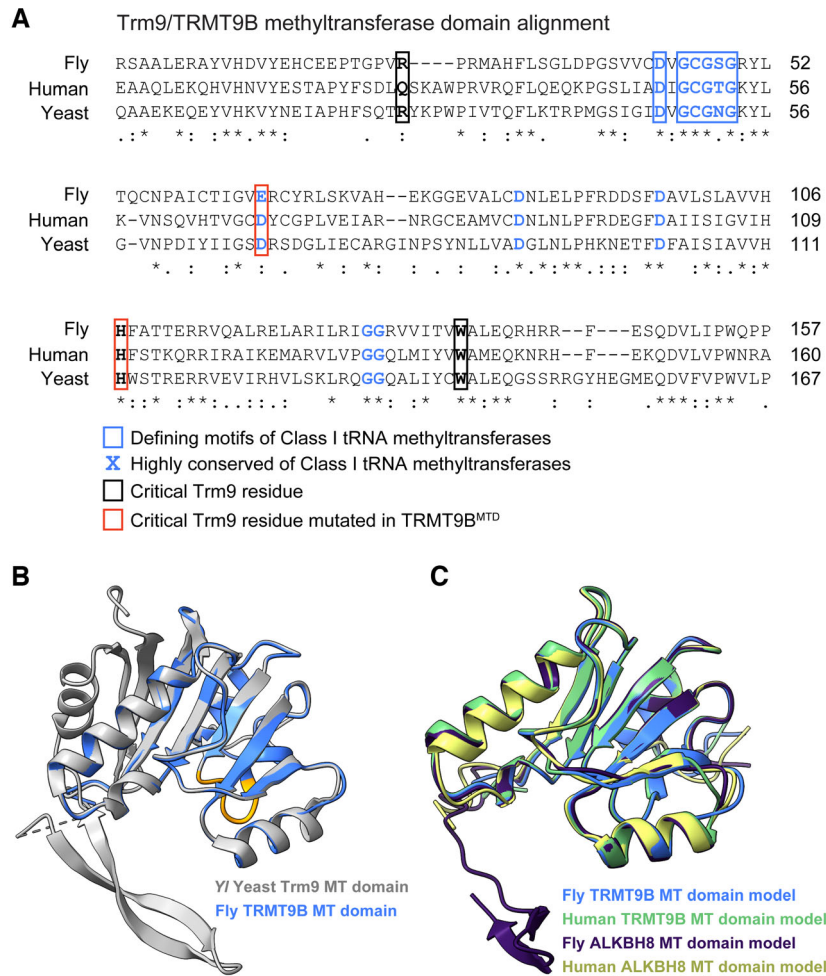
A Trm9/TRMT9B methyltransferase domain alignment

Figure 6. TRMT9B encodes a conserved methyltransferase.

A Sequence alignment of yeast Trm9, *Drosophila* TRMT9B, and human TRMT9B methyltransferase domains. Class I methyltransferase defining sequences are blue and boxed. Additional residues highly conserved across class I methyltransferases are indicated in blue. Critical residues identified in yeast by Létoquart *et al* (2015) are boxed in black or red, with red indicating the amino acids mutated in our methyltransferase-dead transgene. Identical amino acids are marked with asterisks, conserved substitutions are marked with two dots, and semiconserved substitutions with single dots.

B Structural homology model of the *Drosophila* TRMT9B methyltransferase domain (blue) with yeast Trm9 structure (gray, PBD ID: 5CM2 chain Z). The class I methyltransferase GxGxG motif (orange) is in conserved positions across species.

C Extension of the homology model shows conserved tertiary structure between *Drosophila* (blue) and human (green) TRMT9B and *Drosophila* (purple) and human (yellow) ALKBH8 methyltransferase domains.

methyltransferase-dead TRMT9B, we generated V5-tagged versions of both transgenes and confirmed expression of the correct size proteins at comparable levels by western blot (Fig EV5A and B) and similar localization patterns when expressed in neurons or muscle (Fig EV5C–H). Consistent with our sequence and structural analyses, these data provide additional support for the model that TRMT9B functions through a methyltransferase-dependent mechanism to regulate synaptic growth.

TRMT9B regulates neurotransmitter release through a distinct mechanism

Our findings indicate that TRMT9B promotes neurotransmitter release independently of its role in regulating synapse number. To determine whether methyltransferase function is also required for

TRMT9B's role in neurotransmission, we first conducted cell-specific rescue and found that postsynaptic expression of *TRMT9B* fully rescues neurotransmitter release (Fig 8A–D and H–J). In contrast, presynaptic expression of TRMT9B fails to rescue ($TRMT9B^{KO/HA+IC}$ vs. *C155*; $TRMT9B^{KO}/UAS\text{-}TRMT9B$, $TRMT9B^{HA+IC}$: $P = 0.408$, ANOVA followed by Tukey's test). We next attempted to rescue synaptic function with $TRMT9B^{MTD}$ and found that methyltransferase-dead TRMT9B also restores neurotransmitter release (Fig 8E and H–J). We assessed neurotransmission upon postsynaptic overexpression of either methyltransferase-dead or wild-type TRMT9B and observed no effect (Fig 8F–J), ruling out additive effects. Thus, TRMT9B can promote neurotransmitter release independently of its methyltransferase function. These findings indicate diverse functions for TRMT9B in synaptogenesis and neurotransmitter release and underscore the important
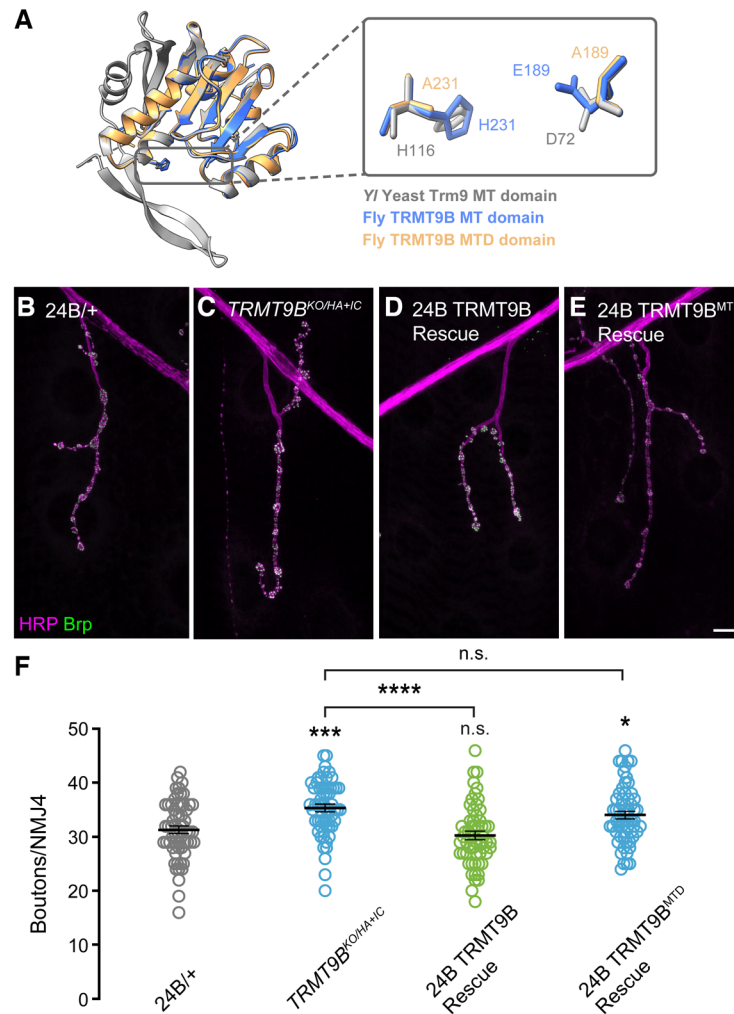
Figure 7. TRMT9B regulation of synaptic growth requires methyltransferase function.

A   Homology model of TRMT9B with methyltransferase-disrupting mutations. Superimposition of wild-type (blue) and methyltransferase-dead (MTD, light orange) TRMT9B methyltransferase domain models with yeast Trm9 structure (gray, PBD ID: 5CM2 chain Z) indicates the preservation of tertiary structure in TRMT9B^MTD. Insert shows mutated residues in TRMT9B^MTD.

B–E   Representative confocal images of NMJ4 in control (gray), *TRMT9B* null (blue), postsynaptic TRMT9B rescue (green), and postsynaptic TRMT9B^MTD rescue (blue). Scale bar: 10 μm.

F   Quantification of bouton number per NMJ4 from B-E. Data points represent individual NMJs (*24B-Gal4/+*: 60, *24B-Gal4, TRMT9B^KO/HA+IC*: 59; *24B-Gal4, TRMT9B^KO/ UAS-TRMT9B, TRMT9B^HA+IC*: 57; *24B-Gal4, TRMT9B^KO/UAS-TRMT9B^MTD, TRMT9B^HA+IC*) from 10 biological replicates per genotype. Mean ± S.E.M. is indicated. ANOVA followed by Tukey's multiple comparisons test. ****$P < 0.0001$, ***$P = 0.0003$, *$P = 0.03$.

role of the expanded metazoan tRNA methyltransferase family in the nervous system.

Discussion

We hypothesized that we could identify new, conserved regulators of synapse formation among uncharacterized genes whose transcription specifically correlates with peak periods of synaptogenesis during *Drosophila* embryonic and adult nervous system development. This otherwise unbiased approach led to the surprise discovery of a member of the tRNA methyltransferase family. Through biochemical, structural modeling and genetic studies, we found that

TRMT9B regulates synaptogenesis through a methyltransferase-dependent mechanism and may have evolved in animals to methylate a novel substrate. Our data also suggest that TRMT9B can promote neurotransmitter release through a nonenzymatic mechanism. These findings highlight both the important regulatory role of methylation in the nervous system and the expanding functions of tRNA methyltransferase family members.

In *Drosophila*, *TRMT9B* transcription peaks in late embryogenesis shortly before synaptogenesis begins in the developing nervous system. *TRMT9B* is primarily expressed in the nervous system, with lower levels of expression in carcass (muscle and epidermis), fat body, imaginal disks, and testes (Brown *et al*, 2014). Similarly, mouse and human *TRMT9B* are highly expressed in the nervous
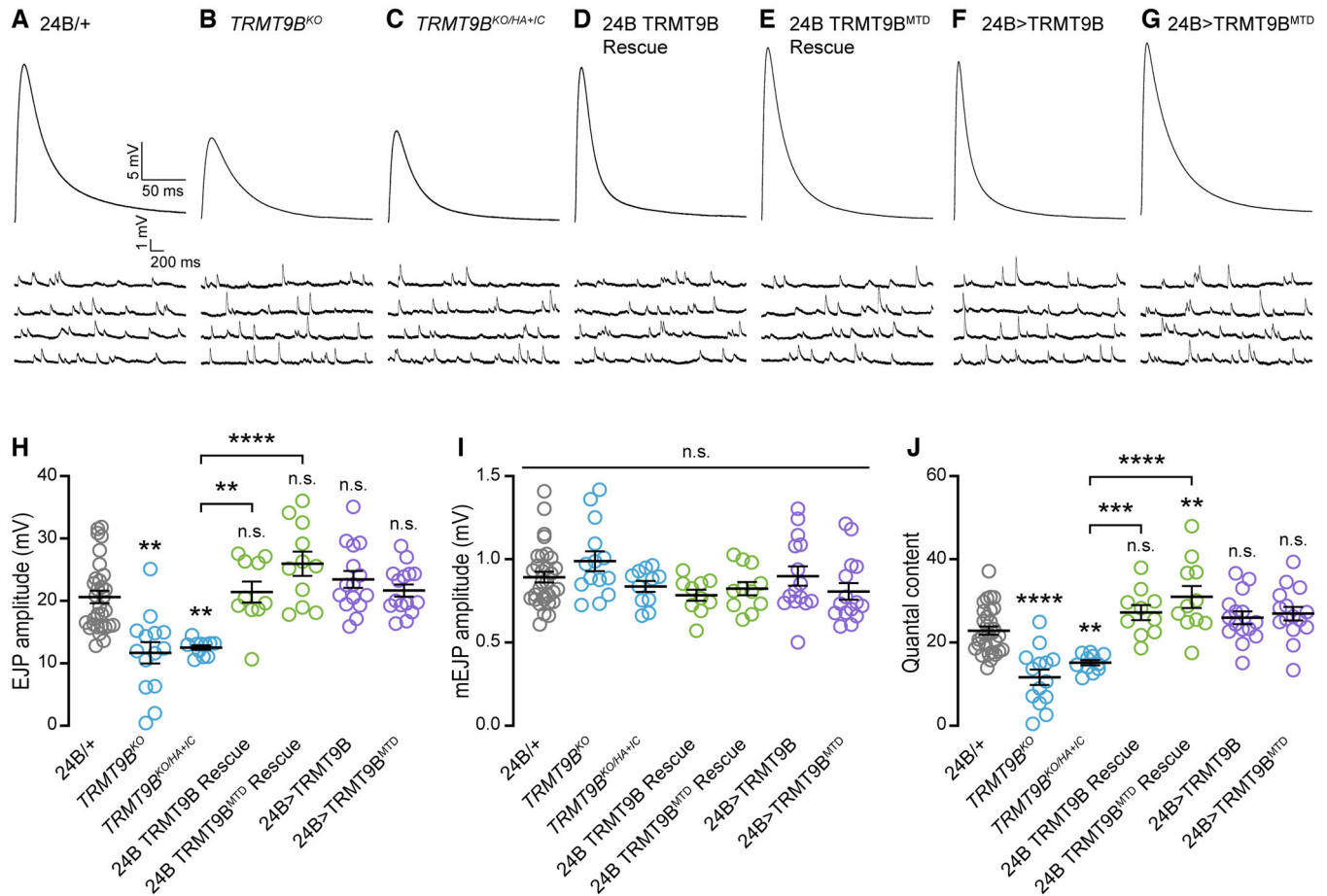
Figure 8. TRMT9B regulates neurotransmitter release through a distinct mechanism.

A-G Representative traces of EJPs and mEJPs from current clamp recordings at muscle 6 in control (gray), two *TRMT9B* null alleles (blue), TRMT9B and TRMT9B[MTD] rescue (green), and overexpression (purple). Stimulus artifacts have been removed from EJPs for clarity.

H–J Quantification of average mEJP amplitude, EJP amplitude, and quantal content for genotypes in A-G. Data points represent individual NMJs (*24B-Gal4/+*: 31, *TRMT9B[KO]*: 14, TRMT9B[KO/HA+IC]: 11; *24B-Gal4, TRMT9B[KO]/UAS-TRMT9B, TRMT9B[HA+IC]*: 10; *24B-Gal4, TRMT9B[KO]/UAS-TRMT9B[MTD], TRMT9B[HA+IC]*: 11; *24B-Gal4/UAS-TRMT9B*: 15; *24B-Gal4/UAS-TRMT9B[MTD]*: 15) from 4 to 11 biological replicates per genotype. Mean ± S.E.M. is indicated. Kruskal–Wallis nonparametric test followed by Dunn's multiple comparisons test for EJPs and mEJPs. ANOVA followed by Tukey's test for normally distributed QC. ****$P < 0.0001$, ***$P < 0.001$, **$P < 0.01$.

system, including the cerebellum, visual cortex, hippocampus, and cerebral cortex (Yue *et al*, 2014; GTEx, 2015; Uhlén *et al*, 2015). Nonetheless, to date TRMT9B has only been studied in the context of non-neuronal cancers, although a recent study found that TRMT9B expression is significantly increased along with a host of gene regulatory proteins during NeuroD1-mediated conversion of astrocytes to neurons (Ma *et al*, 2022). An RNAi screen in *Drosophila* identified a putative role for *Drosophila TRMT9B* in promoting dendrite outgrowth in class IV multidendritic sensory neurons and in thermal nociception (Honjo *et al*, 2016). We find that TRMT9B negatively regulates synaptogenesis at the NMJ and *TRMT9B* mutants display significant impairment in neurotransmitter release. While bouton number is increased in *TRMT9B* mutants, a homeostatic decrease in the number of active zones per bouton normalizes synapse number per NMJ. This indicates that abnormal synaptic transmission in *TRMT9B* mutants is due to functional impairment of the individual synapses that compose the NMJ rather than altered synapse number,

pointing to a requirement for TRMT9B in regulating both NMJ development and the formation of functional synapses.

In 2004, TRMT9B was first identified as a potential tumor suppressor in colorectal cancer (Flanagan *et al*, 2004). Since that time, reduced TRMT9B expression due to genomic rearrangements or epigenetic silencing has been observed in ovarian, lung, and other carcinomas (Flanagan *et al*, 2004; Begley *et al*, 2013; Chen *et al*, 2017; Wang *et al*, 2018). Restoration of TRMT9B expression in colon, lung, and ovarian cancer cells reduces proliferation and significantly reduces colon tumor growth *in vivo*, confirming an important tumor suppressor role for TRMT9B (Blanco *et al*, 2014; Chen *et al*, 2017; Wang *et al*, 2018). Despite the numerous links to cancer, the biological role of TRMT9B function has remained unknown. Although insight into TRMT9B's biochemical role has been limited by the lack of an animal model, a gain-of-function study found that TRMT9B promotes the expression of tumor suppressor LIN9, a core member of the DREAM complex that represses cell cycle-dependent gene

expression, and blocks HIF1-α-dependent adaptation to hypoxia (Begley *et al*, 2013). A more recent study found that stress-dependent phosphorylation modulates TRMT9B's interactions with the 14-3-3 gamma, epsilon, and eta signaling molecules and its ability to suppress proliferation and hypoxic adaptation (Gu *et al*, 2018).

The tRNA methyltransferase family of enzymes has expanded from 18 proteins that form 15 holoenzymes in yeast to 34 homologs in humans, with all yeast tRNA methyltransferases represented in animals and more than half represented by two or more paralogs in humans (Towns & Begley, 2012). Many of the additional family members in animals are yet to be characterized, raising the question of whether they maintain redundant roles as canonical tRNA methyltransferases or have evolved new functions. Of the two metazoan homologs of yeast Trm9, mammalian ALKBH8 has been shown to methylate tRNA wobble uridines (Kalhor & Clarke, 2003; Songe-Moller *et al*, 2010; Fu *et al*, 2010a). Our quantitative mass spectrometry studies demonstrate that ALKBH8 is similarly responsible for the methylation of tRNA wobble uridines in *Drosophila*. Notably, ALKBH8 has recently been linked to intellectual disability in several families, suggesting an important role for tRNA wobble uridine methylation in nervous system development (Monies *et al*, 2019; Saad *et al*, 2021; Maddirevula *et al*, 2022).

In contrast, we find that TRMT9B is either dispensable for tRNA wobble uridine methylation or plays a conditional role not detected in our analysis. Our findings are consistent with the previous observation that ALKBH8, but not TRMT9B, can rescue tRNA methylation in a yeast deletion of Trm9 (Begley *et al*, 2013) and suggest TRMT9B may have evolved a new function. TRMT9B might also function as a tRNA wobble uridine methyltransferase under specific conditions or methylate only one or a few, possibly brain-enriched, tRNAs as has recently been demonstrated for a mammalian homolog of yeast Trm140, which methylates tRNAs in the anticodon loop (Xu *et al*, 2017). This possibility would be consistent with the recent finding that overexpression of TRMT9B leads to subtle, but significant changes in tRNAs with an mcm5U terminal modification, although mcm5S2U levels remain unchanged (Jungfleisch *et al*, 2022).

To explore how TRMT9B might function biochemically, we investigated TRMT9B's sequence and structural homology with SAM-dependent methyltransferases. Several lines of evidence suggest that TRMT9B retains methyltransferase function: (i) residues required for enzymatic function in yeast are highly conserved, including the canonical Class I SAM-dependent methyltransferase GxGxG motif and acidic amino acid at the end of the second beta strand, both of which mediate SAM binding; (ii) structural modeling reveals remarkable similarity between the methyltransferase domains of yeast Trm9 and fly and human TRMT9B and ALKBH8; and (iii) disruption of two residues critical for methyltransferase function in yeast eliminates the ability of a *TRMT9B* transgene to rescue synaptic growth without disrupting its ability to fold or localize properly. Although these highly conserved residues appear to be critical for methyltransferase function in *Drosophila TRMT9B*, without a substrate we cannot confirm this biochemically. In contrast to synaptic growth, we found that *TRMT9B^MTD^* restores neurotransmitter release in *TRMT9B* mutants. Thus, TRMT9B appears to have evolved an entirely novel methyltransferase-independent role, possibly as a scaffolding protein or competitive interactor of TRMT112.

Future genetic and biochemical studies to identify functional interactors will be important.

Another major next step will be identifying TRMT9B's substrate(s). A previous study identified changes to a number of tRNA modifications upon expression of TRMT9B (Begley *et al*, 2013). However, it is unclear whether any of these modifications are direct targets of TRMT9B as many tRNA modifications depend on prior modifications. To investigate the possibility that TRMT9B catalyzes a distinct modification on tRNAs, we assessed a panel of tRNA post-transcriptional modifications in our mutants via quantitative mass spectrometry. We did not identify a TRMT9B-dependent modification among our panel, which includes nine of the 12 modifications affected in the Begley *et al* (2013) study. However, it remains possible that TRMT9B catalyzes a modification we were unable to evaluate, including an animal-specific tRNA modification yet to be identified. As most of our understanding of tRNA methylation comes from studies in single-cell organisms, it would not be surprising if additional tRNA modifications specific to animals and possibly enriched in specific tissues such as the nervous system, remain undiscovered. Another possibility is that TRMT9B methylates a non-tRNA substrate. In fact, several members of the expanded metazoan tRNA methyltransferase family methylate non-tRNA substrates. For example, the NSUN family of yeast Trm4 homologs methylate not only tRNAs but also mRNA, rRNA, and noncoding RNAs and have important roles in both cancer and neurodevelopment (Abbasi-Moheb *et al*, 2012; Chellamuthu & Gray, 2020; Chen *et al*, 2021). Intriguingly, we have found that both fly and human TRMT9B immunoprecipitate TRMT112, the homolog of obligate yeast Trm9 cofactor Trm112, in IP-LC-MS/MS experiments (two unique peptides, 11% peptide coverage; (Gu *et al*, 2018), respectively). TRMT112 promotes the methylation of diverse substrates as an obligate cofactor for several tRNA, rRNA, and protein methyltransferases—an indication of the expansive landscape of potential TRMT9B substrates (Guy & Phizicky, 2014; van Tran *et al*, 2019; Gao *et al*, 2020; Garcia *et al*, 2021; Yang *et al*, 2021). A recent study of the Trm112 interactome in Archaea identified a similarly broad array of interacting methyltransferases as well as small molecule methyltransferases involved in steroid and vitamin biosynthesis (van Tran *et al*, 2018), raising still more diverse possibilities. Especially exciting is the possibility, hinted at by its endogenous expression pattern, that TRMT9B methylates distinct targets in different cellular and subcellular contexts, including synaptic targets. Given TRMT9B's fundamental roles as a regulator of synapse formation and function and a tumor suppressor, it will be of great interest and clinical significance to identify target(s) of TRMT9B methylation in future studies.

Materials and Methods

Drosophila genetics and gene editing

The following stocks used in this study are available through the Bloomington Drosophila Stock Center (BDSC): *w^1118^* (RRID:BDSC_5905), *vasa-Cas9* (RRID:BDSC_51324), piggyBac transposase (RRID:BDSC_8283), *attP2* (RRID:BDSC_25710), *elav^c155^ Gal4* (RRID:BDSC_458), *24B Gal4* (RRID:BDSC_92172). *y^1^ w*; Mi{MIC}fid^MI13909^* (*TRMT9B MiMIC^Stop^*) and *y^1^ w*; Mi{PT-GFSTF.1}*

dfid[MI13909-GFSTF.1] (*TRMT9B MiMIC*[GFP]) were generated through the Gene Disruption Project and obtained from the BDSC (RRID: BDSC_59229 and RRID:BDSC_66771; Nagarkar-Jaiswal *et al*, 2015; Venken *et al*, 2011). All crosses were set up with 10 males and 10 females in 25°C incubators with humidity control and 12-h light/dark cycles.

CRISPR-based homology-directed repair strategies were used to generate knockouts and in-frame endogenous tags. Target sites were selected using CRISPR Optimal Target Finder program (http://targetfinder.flycrispr.neuro.brown.edu; Gratz *et al*, 2014). The following gRNAs were used: TRMT9B[KO]: 5′-AATCCATCGTCCTGAAAT AG-3′, 5′-AGTCTATTACTCTAGTCGGC-3′; TRMT9B[HA+IC]: 5′-CGACGGCTTTGTTGAATGCG-3′. gRNA and donor plasmids were generated as described in (Gratz *et al*, 2014). *Vasa-Cas9* embryos were injected with a mixture of two gRNA plasmids (100 ng/µl, each) and a double-stranded DNA donor plasmid (500 ng/µl) by BestGene, Inc., crossed to *w*[1118] flies after eclosion, and progeny screened for DsRed expression in the eye. Knockout alleles were generated by replacing the majority of the endogenous locus with a visible marker and attP landing site (Gratz *et al*, 2013). Endogenously tagged alleles were created using a scarless CRISPR-piggyBac approach (https://flycrispr.org; Bruckner *et al*, 2017; Gratz *et al*, 2019). An HA or superfolder GFP (sfGFP) tag flanked by flexible linkers and a visible marker flanked by piggyBac inverted terminal repeat sequences were inserted immediately downstream of the sole *TRMT9B* or ALKBH8 (CG17807) translational start sites. This generates null alleles due stop codons in the inverted repeat sequences. TRMT9B lines were crossed to piggyBac transposase to remove the marker cassette and generate in-frame tags. All engineered lines were confirmed by PCR and Sanger sequencing.

UAS rescue lines were generated by cloning full-length *Drosophila* and human TRMT9B coding sequence into pUAST-C5 (*Drosophila* Genomics Resource Center #1261). To generate methyltransferase-dead *Drosophila* TRMT9B, mutations to critical residues in the methyltransferase domain were introduced via KLD reaction. Specifically, we mutated codon 417 (GAG to GCC) and codon 693 (CAC to GCC) to introduce E139A and H231A mutations. These amino acids correspond to yeast residues D72 and H116, which were identified as critical for methyltransferase function (Létoquart *et al*, 2015). In parallel, we generated V5-tagged wild-type and methyltransferase-dead *Drosophila TRMT9B* transgenes to confirm localization. All transgenes were integrated into the attP2 landing site by BestGene, Inc. (Groth *et al*, 2004).

Immunostaining and confocal imaging

Male third-instar larvae were dissected in Ca^{2+}-free saline and fixed for 10 min with 4% paraformaldehyde in PBS. Dissected larvae were washed and permeabilized in PBS with 0.1% Triton X and then blocked overnight at 4°C in PBS containing 0.1% Triton X and 1% BSA. Dissected larvae were incubated with primary antibodies for 2 h at room temperature and secondary antibodies for 1 h at room temperature and then mounted in Vectashield (Vector Laboratories). For localization studies, male third-instar larvae were dissected in ice-cold Ca^{2+}-free saline and fixed for 6 min in Bouin's Fixative. Dissected larvae were washed and permeabilized in PBS with 0.1% Triton X and then blocked overnight at 4°C in PBS containing 0.1% Triton X, 5% NGS, and 1% BSA, followed by

overnight incubation with primary and secondary antibodies and then mounted in Vectashield (Vector Laboratories). The following antibodies were used at the indicated concentrations: mouse anti-Bruchpilot (Brp) at 1:100 (Developmental Studies Hybridoma Bank (DSHB) #nc82; RRID: AB_2314866), rabbit anti-HA at 1:500 (Cell Signaling Technology C29F4), mouse anti-V5 (1:500, ThermoFisher Scientific #R960-25; RRID:AB_2556564), anti-HRP conjugated to Alexa Fluor 647 at 1:500 (Jackson ImmunoResearch Laboratories, Inc., #123–605-021; RRID:AB_2338967), rabbit anti-GFP conjugated to AlexaFluor 488 at 1:500 (Thermo Fisher Scientific, #A-21311; RRID:AB_221477), and secondary antibodies Alexa Fluor 488, Alexa Fluor 568, and Alexa Fluor 647 at 1:500 (Thermo Fisher Scientific). Images were obtained on a Nikon A1R HD confocal microscope with Plan Apo 40× and 60× oil-immersion objectives.

Electrophysiology

Electrophysiological baseline readings were performed on male third-instar larvae. Larvae were dissected in low Ca^{2+} modified hemolymph-like saline (HL3: 70 mM NaCl, 5 mM KCl, 20 mM $MgCl_2$, 10 mM $NaHCO_3$, 115 mM sucrose, 5 mM trehalose, 5 mM HEPES, and 0.2 mM Ca^{2+}, pH 7.2). Excitatory junction potentials were recorded using 1.0 mm × 0.58 mm, 4″ borosilicate glass sharp electrode (electrode resistance between 10 and 15 MΩ) filled with 3 M KCl. Recordings were performed in hemolymph-like saline solution containing 0.6 mM Ca^{2+} on muscle 6 of abdominal segments A3 and A4. A 1.5 mm × 1.12 mm, 4″ borosilicate polished glass electrode was used to suction nerves. Recordings were performed on a Nikon FN1 microscope using a 40× (0.80 NA) water-dipping objective and acquired using an AxoClamp 900A amplifier, Axon Digidata 1550B low-noise data acquisition system, and pClamp 11.0.3 software (Molecular Devices). Electrophysiological sweeps were digitized at 10 kHz and filtered at 0.1 kHz. Miniature excitatory junctional potentials (mEJPs) were recorded with no external stimulation. For each recording, at least 100 mEJPs were analyzed using Mini Analysis (Synaptosoft) to obtain a mean mEJP amplitude value per muscle. Cut motor axons of each segment were stimulated for 0.5 ms with an A-M Systems Isolated pulse stimulator to elicit EJPs. Stimulus intensity was adjusted to consistently elicit compound responses from both type Ib and Is motor neurons. At least 30 consecutive EJPs were recorded for each cell and analyzed in pClamp to obtain mean amplitude. Quantal content (QC) was determined for each recording by calculating the ratio of mean EJP amplitude to mean mEJP amplitude and then averaging recordings across all NMJs for a given genotype. Muscle input resistance (Rin) and resting membrane potential (V_{rest}) were monitored during each experiment. Recordings were only performed if the V_{rest} was between −50 and −80 mV and membrane resistance was 4 MΩ or higher.

Sequence alignment, phylogeny, and homology modeling

Alignments of the methyltransferase domains as defined by Pfam (Mistry *et al*, 2021) were conducted using T-Coffee (Notredame *et al*, 2000) using the following UniProt sequences: P49957 (*Saccharomyces cerevisiae* Trm9), Q9VBJ3 (*Drosophila* TRMT9B), Q9P272 (human TRMT9B), Q9W232 (*Drosophila* ALKBH8), and Q96BT7 (human ALKBH8). A phylogenetic tree was determined by PhyML

maximum likelihood and visualized with TreeDyn in phylogeny.fr (Dereeper *et al*, 2008; Lemoine *et al*, 2019). Template-based structural homology models of the methyltransferase domains of *Drosophila* and human TRMT9B and ALKBH8 were performed using Modeller (Pieper *et al*, 2014) through the ModWeb online service (https://modbase.compbio.ucsf.edu/modweb). Best scoring models for all four proteins included *Yarrowia lipolytica* Trm9, obtained from 2.5 Å X-ray diffraction of Trm9-Trm112, PDB: 5CM2 chain Z (Létoquart *et al*, 2015). All homology models built with PDB 5CM2 chain Z were reliable with GA341 score of > 0.99989 and normalized DOPE (zDOPE) score < 0. *Drosophila* and human TRMT9B models were built with residues 39–160 of *Y. lipolytica*, with 39 and 46% sequence identity, respectively. The *Drosophila* ALKBH8 model was built with residues 39–191 with 40% sequence identity and the human ALKBH8 model was built with residues 16–174 with 46% sequence identity. To model the mutations in methyltransferase-dead TRMT9B, we again used residues 39–160. Additional details on the best scoring models can be found in the associated protein data bank files (Source data, Harvard Dataverse). Models were visualized and compared with PDB 5CM2 chain Z using UCSF ChimeraX (Pettersen *et al*, 2021). A template-free model for *Drosophila* TRMT9B was obtained from AlphaFold version 1 predictions (see Source data, Harvard Dataverse; Jumper *et al*, 2021; Varadi *et al*, 2022). The AlphaFold model confidently predicted (pLDDT > 70) the methyltransferase domain, residues 123–278, although a biological function was not defined. Confidence scores for critical methyltransferase activity including the GxGxG domain, the acidic residue, and SAM-binding histidine were very high (pLDDT between 89.8 and 95.7).

Liquid chromatography-mass spectrometry of RNA modifications

Vials containing adult fly heads were flash-frozen in liquid nitrogen and stored at −80°C. Twenty-five milligrams of frozen adult flies were homogenized with a plastic pestle in a 1.5 ml microfuge tube while adding 250 µl of TRIzol reagent at a time until 1 ml was added. RNA was then extracted via an adapted TRIzol extraction protocol (Bogart & Andrews, 2006). RNA was resuspended in RNase-free ddH$_2$O. Total RNA was processed and analyzed by LC–MS as previously described (Su *et al*, 2014; Zhang *et al*, 2020). Briefly, total RNA (20 µg) was digested and dephosphorylated with benzonase, phosphodiesterase, and calf-intestinal phosphatase for 3 h at 37°C. Enzymes and undigested RNAs were removed using a 10,000-Da MWCO spin filter (Amicon), and purified ribonucleosides were stored at −80°C until further analysis. For fly larval preparations, wandering third-instar larvae were dissected in HL3 with RNAse and paraformaldehyde free tools. The CNS and body walls were manually homogenized with a plastic pestle in 200uL TRIzol reagent, frozen and stored at −80°C before extraction using the Direct-zol RNA micropep kit (Zymo Research), and processed as described above. Ribonucleosides were separated using a Hypersil GOLD™ C18 Selectivity Column (Thermo Scientific) followed by nucleoside analysis using a Q Exactive Plus Hybrid Quadrupole-Orbitrap. The modification difference ratio was calculated using the m/z intensity values of each modified nucleoside between control and mutants following normalization to the sum of intensity values for the canonical nucleosides A, U, G, and C.

IP-MS analysis of TRMT9B-interacting proteins

We pulled down endogenous TRMT9B protein and interacting proteins in y^1 $w*$; $Mi\{PT\text{-}GFSTF.1\}dfid^{MI13909\text{-}GFSTF.1}$, in which TRMT9B is tagged with GFP and FLAG (Nagarkar-Jaiswal *et al*, 2015). Whole adult flies were flash-frozen in liquid nitrogen and manually homogenized. Cells were then lysed in lysis buffer (50 mM Tris–HCl, pH 7.5, 150 mM NaCl, 1 mM EDTA, 1% Triton X-100 supplemented with a protease inhibitor cocktail). Lysates were cleared by centrifugation and immunoprecipitated with anti-FLAG-antibody-conjugated agarose beads. Beads were washed three times with FLAG-wash buffer (50 mM Tris–HCl, pH 7.5, 500 mM NaCl, 1 mM EDTA, 1% Triton X-100) and twice with TBS buffer (50 mM Tris–HCl, pH 7.5, 150 mM NaCl). EGFP-FIAsH-StrepII-3×FLAG -tagged TRMT9B was eluted with 100 µg/ml of 3×FLAG peptide in TBS buffer. As a control, an identical purification was performed in w1118 control flies. A silver stain was performed to confirm the presence of proteins in the eluted fractions, which were then subjected to trypsin digestion and tandem mass spectrometry. We used a 1% false discovery rate peptide threshold and 99% protein threshold to identify interacting proteins identified by at least two unique peptides.

Western blots

Protein samples were prepared from wandering third-instar larvae in the 2× Laemmli buffer followed by boiling at 95°C for 5 min. The following antibodies were used: mouse anti-V5 (1:5,000, RRID: AB_2556564, ThermoFisher Scientific # R960-25) and mouse anti-tubulin (1:4,000, RRID: AB_2315513, Developmental Studies Hybridoma Bank #E7c). Secondary antibodies (Jackson Immunochemicals) were used at 1:10,000. Quantification was performed using ImageJ software.

Experimental design and statistical analysis

Quantifications were conducted blind to genotype. Sample sizes were based on prior published studies. Statistical analyses were conducted in GraphPad Prism 8 and 9. One-way ANOVA followed by Tukey's test was used for multiple comparisons of normally distributed data with equal variance. Multiple comparisons of non-normally distributed data were performed using the Kruskal–Wallis test followed by Dunn's multiple comparisons test. Significance is reported as values less than 0.05, 0.01, 0.001, and 0.0001 represented by one, two, three, or four stars, respectively. Unless otherwise indicated, significance refers to the indicated genotype compared with control. Error bars represent the mean ± S.E.M. or standard deviation as indicated.

Data availability

Source data for all figures are available at the Harvard Dataverse repository: https://doi.org/10.7910/DVN/2ZDR8P.

Expanded View for this article is available online.

Acknowledgements

Author contributions

Caley A Hogan: Conceptualization; formal analysis; investigation; visualization; writing – original draft; writing – review and editing. **Scott J Gratz:** Conceptualization; formal analysis; investigation; visualization; writing – review and editing. **Jennifer L Dumouchel:** Formal analysis; investigation; visualization; writing – review and editing. **Rajan S Thakur:** Formal analysis; investigation; visualization; writing – review and editing. **Ambar Delgado:** Formal analysis; investigation; writing – review and editing. **Jenna M Lentini:** Formal analysis; investigation; visualization; writing – review and editing. **Kimberly R Madhwani:** Formal analysis; investigation; visualization; writing – review and editing. **Dragony Fu:** Conceptualization; formal analysis; funding acquisition; investigation; visualization; project administration; writing – review and editing. **Kate M O'Connor-Giles:** Conceptualization; formal analysis; funding acquisition; visualization; writing – original draft; project administration; writing – review and editing.

Disclosure and competing interests statement

The authors declare that they have no conflict of interest.

References

Abbasi-Moheb L, Mertel S, Gonsior M, Nouri-Vahid L, Kahrizi K, Cirak S, Wieczorek D, Motazacker MM, Esmaeeli-Nieh S, Cremer K *et al* (2012) Mutations in NSUN2 cause autosomal-recessive intellectual disability. *Am J Hum Genet* 90: 847–855

Begley U, Dyavaiah M, Patil A, Rooney JP, DiRenzo D, Young CM, Conklin DS, Zitomer RS, Begley TJ (2007) Trm9-catalyzed tRNA modifications link translation to the DNA damage response. *Mol Cell* 28: 860–870

Begley U, Sosa MS, Avivar-Valderas A, Patil A, Endres L, Estrada Y, Chan CT, Su D, Dedon PC, Aguirre-Ghiso JA *et al* (2013) A human tRNA methyltransferase 9-like protein prevents tumour growth by regulating LIN9 and HIF1-alpha. *EMBO Mol Med* 5: 366–383

Blanco S, Dietmann S, Flores JV, Hussain S, Kutter C, Humphreys P, Lukk M, Lombard P, Treps L, Popis M *et al* (2014) Aberrant methylation of tRNAs links cellular stress to neuro-developmental disorders. *EMBO J* 33: 2020–2039

Bogart K, Andrews J (2006) Extraction of total RNA from *Drosophila*. CGB Technical Report 2006-10

van den Born E, Vagbo CB, Songe-Moller L, Leihne V, Lien GF, Leszczynska G, Malkiewicz A, Krokan HE, Kirpekar F, Klungland A *et al* (2011) ALKBH8-mediated formation of a novel diastereomeric pair of wobble nucleosides in mammalian tRNA. *Nat Commun* 2: 172

Brown JB, Boley N, Eisman R, May GE, Stoiber MH, Duff MO, Booth BW, Wen J, Park S, Suzuki AM *et al* (2014) Diversity and dynamics of the *Drosophila* transcriptome. *Nature* 512: 393–399

Bruckner JJ, Zhan H, Gratz SJ, Rao M, Ukken F, Zilberg G, O'Connor-Giles KM (2017) Fife organizes synaptic vesicles and calcium channels for high-probability neurotransmitter release. *J Cell Biol* 216: 231–246

Cai WM, Chionh YH, Hia F, Gu C, Kellner S, McBee ME, Ng CS, Pang YL, Prestwich EG, Lim KS *et al* (2015) A platform for discovery and quantification of modified ribonucleosides in RNA: application to stress-induced reprogramming of tRNA modifications. *Methods Enzymol* 560: 29–71

Chellamuthu A, Gray SG (2020) The RNA methyltransferase NSUN2 and its potential roles in cancer. *Cell* 9: 1758

Chen C, Huang B, Anderson JT, Byström AS (2011) Unexpected accumulation of ncm(5)U and ncm(5)S(2) (U) in a trm9 mutant suggests an additional step in the synthesis of mcm(5)U and mcm(5)S(2)U. *PLoS One* 6: e20783

Chen HM, Wang J, Zhang YF, Gao YH (2017) Ovarian cancer proliferation and apoptosis are regulated by human transfer RNA methyltransferase 9-likevia LIN9. *Oncol Lett* 14: 4461–4466

Chen YS, Yang WL, Zhao YL, Yang YG (2021) Dynamic transcriptomic m(5) C and its regulatory role in RNA processing. *Wiley Interdiscip Rev RNA* 12: e1639

Citri A, Malenka RC (2008) Synaptic plasticity: multiple forms, functions, and mechanisms. *Neuropsychopharmacology* 33: 18–41

Dereeper A, Guignon V, Blanc G, Audic S, Buffet S, Chevenet F, Dufayard JF, Guindon S, Lefort V, Lescot M *et al* (2008) Phylogeny.fr: robust phylogenetic analysis for the non-specialist. *Nucleic Acids Res* 36: W465–W469

Dewe JM, Fuller BL, Lentini JM, Kellner SM, Fu D (2017) TRMT1-catalyzed tRNA modifications are required for redox homeostasis to ensure proper cellular proliferation and oxidative stress survival. *Mol Cell Biol* 37: e00214-17

Flanagan JM, Healey S, Young J, Whitehall V, Trott DA, Newbold RF, Chenevix-Trench G (2004) Mapping of a candidate colorectal cancer tumor-suppressor gene to a 900-kilobase region on the short arm of chromosome 8. *Genes Chromosomes Cancer* 40: 247–260

Fu D, Brophy JA, Chan CT, Atmore KA, Begley U, Paules RS, Dedon PC, Begley TJ, Samson LD (2010a) Human AlkB homolog ABH8 Is a tRNA methyltransferase required for wobble uridine modification and DNA damage survival. *Mol Cell Biol* 30: 2449–2459

Fu Y, Dai Q, Zhang W, Ren J, Pan T, He C (2010b) The AlkB domain of mammalian ABH8 catalyzes hydroxylation of 5-methoxycarbonylmethyluridine at the wobble position of tRNA. *Angew Chem Int Ed Engl* 49: 8885–8888

Gao J, Wang B, Yu H, Wu G, Wan C, Liu W, Liao S, Cheng L, Zhu Z (2020) Structural insight into HEMK2-TRMT112-mediated glutamine methylation. *Biochem J* 477: 3833–3838

Garcia BCB, Horie M, Kojima S, Makino A, Tomonaga K (2021) BUD23-TRMT112 interacts with the L protein of Borna disease virus and mediates

the chromosomal tethering of viral ribonucleoproteins. *Microbiol Immunol* 65: 492–504

Goel P, Dufour Bergeron D, Bohme MA, Nunnelly L, Lehmann M, Buser C, Walter AM, Sigrist SJ, Dickman D (2019) Homeostatic scaling of active zone scaffolds maintains global synaptic strength. *J Cell Biol* 218: 1706–1724

Gratz SJ, Goel P, Bruckner JJ, Hernandez RX, Khateeb K, Macleod GT, Dickman D, O'Connor-Giles KM (2019) Endogenous tagging reveals differential regulation of Ca^{2+} channels at single AZs during presynaptic homeostatic potentiation and depression. *J Neurosci* 39: 2416–2429

Gratz SJ, Wildonger J, Harrison MM, O'Connor-Giles KM (2013) CRISPR/Cas9-mediated genome engineering and the promise of designer flies on demand. *Fly* 7: 249–255

Gratz SJ, Ukken FP, Rubinstein CD, Thiede G, Donohue LK, Cummings AM, O'Connor-Giles KM (2014) Highly specific and efficient CRISPR/Cas9-catalyzed homology-directed repair in Drosophila. *Genetics* 196: 961–971

Graveley BR, Brooks AN, Carlson JW, Duff MO, Landolin JM, Yang L, Artieri CG, van Baren MJ, Boley N, Booth BW *et al* (2011) The developmental transcriptome of *Drosophila melanogaster*. *Nature* 471: 473–479

Greenberg MVC, Bourc'his D (2019) The diverse roles of DNA methylation in mammalian development and disease. *Nat Rev Mol Cell Biol* 20: 590–607

Groth AC, Fish M, Nusse R, Calos MP (2004) Construction of transgenic *Drosophila* by using the site-specific integrase from phage phiC31. *Genetics* 166: 1775–1782

GTEx (2015) Human genomics. The Genotype-Tissue Expression (GTEx) pilot analysis: multitissue gene regulation in humans. *Science* 348: 648–660

Gu C, Ramos J, Begley U, Dedon PC, Fu D, Begley TJ (2018) Phosphorylation of human TRM9L integrates multiple stress-signaling pathways for tumor growth suppression. *Sci Adv* 4: eaas9184

Guang S, Pang N, Deng X, Yang L, He F, Wu L, Chen C, Yin F, Peng J (2018) Synaptopathology involved in autism spectrum disorder. *Front Cell Neurosci* 12: 470

Guy MP, Phizicky EM (2014) Two-subunit enzymes involved in eukaryotic post-transcriptional tRNA modification. *RNA Biol* 11: 1608–1618

Honjo K, Mauthner SE, Wang Y, Skene JH, Tracey WD Jr (2016) Nociceptor-enriched genes required for normal thermal nociception. *Cell Rep* 16: 295–303

Johansson MJ, Esberg A, Huang B, Bjork GR, Bystrom AS (2008) Eukaryotic wobble uridine modifications promote a functionally redundant decoding system. *Mol Cell Biol* 28: 3301–3312

Jumper J, Evans R, Pritzel A, Green T, Figurnov M, Ronneberger O, Tunyasuvunakool K, Bates R, Žídek A, Potapenko A *et al* (2021) Applying and improving AlphaFold at CASP14. *Proteins* 89: 1711–1721

Jungfleisch J, Bottcher R, Tallo-Parra M, Perez-Vilaro G, Merits A, Novoa EM, Diez J (2022) CHIKV infection reprograms codon optimality to favor viral RNA translation by altering the tRNA epitranscriptome. *Nat Commun* 13: 4725

Kalhor HR, Clarke S (2003) Novel methyltransferase for modified uridine residues at the wobble position of tRNA. *Mol Cell Biol* 23: 9283–9292

Kozbial PZ, Mushegian AR (2005) Natural history of S-adenosylmethionine-binding proteins. *BMC Struct Biol* 5: 19

Lemoine F, Correia D, Lefort V, Doppelt-Azeroual O, Mareuil F, Cohen-Boulakia S, Gascuel O (2019) NGPhylogeny.fr: new generation phylogenetic services for non-specialists. *Nucleic Acids Res* 47: W260–w265

Létoquart J, van Tran N, Caroline V, Aleksandrov A, Lazar N, van Tilbeurgh H, Liger D, Graille M (2015) Insights into molecular plasticity in protein complexes from Trm9-Trm112 tRNA modifying enzyme crystal structure. *Nucleic Acids Res* 43: 10989–11002

Ma NX, Puls B, Chen G (2022) Transcriptomic analyses of NeuroD1-mediated astrocyte-to-neuron conversion. *Dev Neurobiol* 82: 375–391

Maddirevula S, Alameer S, Ewida N, de Sousa MML, Bjoras M, Vagbo CB, Alkuraya FS (2022) Insight into ALKBH8-related intellectual developmental disability based on the first pathogenic missense variant. *Hum Genet* 141: 209–215

Martin JL, McMillan FM (2002) SAM (dependent) I AM: the S-adenosylmethionine-dependent methyltransferase fold. *Curr Opin Struct Biol* 12: 783–793

Mistry J, Chuguransky S, Williams L, Qureshi M, Salazar GA, Sonnhammer ELL, Tosatto SCE, Paladin L, Raj S, Richardson LJ *et al* (2021) Pfam: the protein families database in 2021. *Nucleic Acids Res* 49: D412–D419

Monies D, Vagbo CB, Al-Owain M, Alhomaidi S, Alkuraya FS (2019) Recessive truncating mutations in ALKBH8 cause intellectual disability and severe impairment of wobble uridine modification. *Am J Hum Genet* 104: 1202–1209

Murn J, Shi Y (2017) The winding path of protein methylation research: milestones and new frontiers. *Nat Rev Mol Cell Biol* 18: 517–527

Nagarkar-Jaiswal S, DeLuca SZ, Lee PT, Lin WW, Pan H, Zuo Z, Lv J, Spradling AC, Bellen HJ (2015) A genetic toolkit for tagging intronic MiMIC containing genes. *eLife* 4: e08469

Notredame C, Higgins DG, Heringa J (2000) T-Coffee: a novel method for fast and accurate multiple sequence alignment. *J Mol Biol* 302: 205–217

Pettersen EF, Goddard TD, Huang CC, Meng EC, Couch GS, Croll TI, Morris JH, Ferrin TE (2021) UCSF ChimeraX: structure visualization for researchers, educators, and developers. *Protein Sci* 30: 70–82

Pieper U, Webb BM, Dong GQ, Schneidman-Duhovny D, Fan H, Kim SJ, Khuri N, Spill YG, Weinkam P, Hammel M *et al* (2014) ModBase, a database of annotated comparative protein structure models and associated resources. *Nucleic Acids Res* 42: D336–D346

Saad AK, Marafi D, Mitani T, Du H, Rafat K, Fatih JM, Jhangiani SN, Coban-Akdemir Z, Baylor-Hopkins Center for Mendelian Genomics, Gibbs RA *et al* (2021) Neurodevelopmental disorder in an Egyptian family with a biallelic ALKBH8 variant. *Am J Med Genet A* 185: 1288–1293

Schaffrath R, Leidel SA (2017) Wobble uridine modifications-a reason to live, a reason to die?! *RNA Biol* 14: 1209–1222

Songe-Moller L, van den Born E, Leihne V, Vagbo CB, Kristoffersen T, Krokan HE, Kirpekar F, Falnes PO, Klungland A (2010) Mammalian ALKBH8 possesses tRNA methyltransferase activity required for the biogenesis of multiple wobble uridine modifications implicated in translational decoding. *Mol Cell Biol* 30: 1814–1827

Stoeger T, Gerlach M, Morimoto RI, Nunes Amaral LA (2018) Large-scale investigation of the reasons why potentially important genes are ignored. *PLoS Biol* 16: e2006643

Su D, Chan CT, Gu C, Lim KS, Chionh YH, McBee ME, Russell BS, Babu IR, Begley TJ, Dedon PC (2014) Quantitative analysis of ribonucleoside modifications in tRNA by HPLC-coupled mass spectrometry. *Nat Protoc* 9: 828–841

Towns WL, Begley TJ (2012) Transfer RNA methyltransferases and their corresponding modifications in budding yeast and humans: activities, predications, and potential roles in human health. *DNA Cell Biol* 31: 434–454

van Tran N, Muller L, Ross RL, Lestini R, Letoquart J, Ulryck N, Limbach PA, de Crecy-Lagard V, Cianferani S, Graille M (2018) Evolutionary insights into Trm112-methyltransferase holoenzymes involved in translation between archaea and eukaryotes. *Nucleic Acids Res* 46: 8483–8499

van Tran N, Ernst FGM, Hawley BR, Zorbas C, Ulryck N, Hackert P, Bohnsack KE, Bohnsack MT, Jaffrey SR, Graille M *et al* (2019) The human 18S rRNA

m6A methyltransferase METTL5 is stabilized by TRMT112. *Nucleic Acids Res* 47: 7719–7733

Tweedie S, Braschi B, Gray K, Jones TEM, Seal RL, Yates B, Bruford EA (2021) Genenames.org: the HGNC and VGNC resources in 2021. *Nucleic Acids Res* 49: D939–d946

Uhlén M, Fagerberg L, Hallström BM, Lindskog C, Oksvold P, Mardinoglu A, Sivertsson Å, Kampf C, Sjöstedt E, Asplund A *et al* (2015) Proteomics. Tissue-based map of the human proteome. *Science* 347: 1260419

Varadi M, Anyango S, Deshpande M, Nair S, Natassia C, Yordanova G, Yuan D, Stroe O, Wood G, Laydon A *et al* (2022) AlphaFold Protein Structure Database: massively expanding the structural coverage of protein-sequence space with high-accuracy models. *Nucleic Acids Res* 50: D439–D444

Venken KJ, Schulze KL, Haelterman NA, Pan H, He Y, Evans-Holm M, Carlson JW, Levis RW, Spradling AC, Hoskins RA *et al* (2011) MiMIC: a highly versatile transposon insertion resource for engineering *Drosophila melanogaster* genes. *Nat Methods* 8: 737–743

Wang S, Liu X, Huang J, Zhang Y, Sang C, Li T, Yuan J (2018) Expression of KIAA1456 in lung cancer tissue and its effects on proliferation, migration and invasion of lung cancer cells. *Oncol Lett* 16: 3791–3795

Xu L, Liu X, Sheng N, Oo KS, Liang J, Chionh YH, Xu J, Ye F, Gao YG, Dedon PC *et al* (2017) Three distinct 3-methylcytidine (m(3)C) methyltransferases modify tRNA and mRNA in mice and humans. *J Biol Chem* 292: 14695–14703

Yang WQ, Xiong QP, Ge JY, Li H, Zhu WY, Nie Y, Lin X, Lv D, Li J, Lin H *et al* (2021) THUMPD3-TRMT112 is a m2G methyltransferase working on a broad range of tRNA substrates. *Nucleic Acids Res* 49: 11900–11919

Yue F, Cheng Y, Breschi A, Vierstra J, Wu W, Ryba T, Sandstrom R, Ma Z, Davis C, Pope BD *et al* (2014) A comparative encyclopedia of DNA elements in the mouse genome. *Nature* 515: 355–364

Zhang K, Lentini JM, Prevost CT, Hashem MO, Alkuraya FS, Fu D (2020) An intellectual disability-associated missense variant in TRMT1 impairs tRNA modification and reconstitution of enzymatic activity. *Hum Mutat* 41: 600–607

Zhou Y, Kong Y, Fan W, Tao T, Xiao Q, Li N, Zhu X (2020) Principles of RNA methylation and their implications for biology and medicine. *Biomed Pharmacother* 131: 110731

Zoghbi HY, Bear MF (2012) Synaptic dysfunction in neurodevelopmental disorders associated with autism and intellectual disabilities. *Cold Spring Harb Perspect Biol* 4: a009886